

Article

A Multi-Flexible-Fingered Roller Pineapple Harvesting Mechanism

Tianhu Liu ^{1,*}, Wei Liu ¹, Tingjun Zeng ², Yifeng Cheng ¹, Yan Zheng ¹ and Jian Qiu ¹¹ College of Engineering, South China Agricultural University, 483 Wushan Road, Guangzhou 510642, China² School of Mechanical and Automotive Engineering, South China University of Technology, 381 Wushan Road, Guangzhou 510640, China

* Correspondence: liuparalake@scau.edu.cn

Abstract: Research on the mechanical harvesting of pineapples is currently in its early stages. The purpose of this study is to provide a design and configure a method for multi-flexible-fingered roller pineapple harvester. Depending on the physical and mechanical characteristics of pineapples, the evaluation function for the critical damage condition of the fruit was established. Our experimental results revealed the optimal parameters for pineapple harvesting were as follows: the rollers of the harvesting mechanism should be inclined at 35°, the left flexible fingers should be 120 mm long, the gap between each of the left flexible fingers should be 30 mm, the length of the right flexible fingers should be 150 mm long, and the gap between each of the right flexible fingers should be 10 mm. The harvesting rate was 85% and the damage rate was 5% in the laboratory; in the natural environment, harvesting rate and damage rate were 78% and 8% respectively, and the harvesting speed was about 1 s per fruit, which demonstrated the harvesting machinery could sufficiently meet the usage demand of pineapple harvesting. In the cases of unsuccessful harvesting, failure resulted from mismatched flexible finger length, fruit size, and harvesting posture and position.



Citation: Liu, T.; Liu, W.; Zeng, T.; Cheng, Y.; Zheng, Y.; Qiu, J. A Multi-Flexible-Fingered Roller Pineapple Harvesting Mechanism. *Agriculture* **2022**, *12*, 1175. <https://doi.org/10.3390/agriculture12081175>

Academic Editor: Rafael-Ruben Sola-Guirado

Received: 20 July 2022

Accepted: 5 August 2022

Published: 7 August 2022

Publisher's Note: MDPI stays neutral with regard to jurisdictional claims in published maps and institutional affiliations.



Copyright: © 2022 by the authors. Licensee MDPI, Basel, Switzerland. This article is an open access article distributed under the terms and conditions of the Creative Commons Attribution (CC BY) license (<https://creativecommons.org/licenses/by/4.0/>).

Keywords: agricultural machinery; mechanism; pineapple harvester; flexible fingers; roller

1. Introduction

The production cost of fruit is high and depends heavily on labor. Most fruits are harvested manually. According to statistics, the cost of hand-harvesting fruits accounts for 30% to 60% of total production cost [1]. The mechanization of fruit harvesting has become increasingly important as the cost of manual labor rises [2]. Competition in the global market requires the use of fast and efficient harvesting systems that reduce harvesting costs. Extensive technical research into fruit and vegetable harvesting machinery has been carried out in various countries [3,4]. There are three main types of mechanized fruit harvesting: harvest-assist platforms, picking robots and mechanized batch harvesting systems [5,6]. Harvest-assist platforms are mainly used to reduce labor intensity and improve manual harvesting efficiency but still require labor. Picking robots and mechanized batch harvesting systems often integrate information from disciplines, such as plant and food sciences, and engineering, in order to reduce labor and simplify the harvesting process [3,4,7]. Most recent studies on picking robots focus on small-sized, light-weight crops [8]. In addition, robotic picking is relatively inefficient, costly and not very stable for long-term use [9,10]. Mechanized batch harvesting methods have been implemented in harvesting nuts and fruits with relatively hard peel since the early 1960s [11–13].

Pineapples play a significant role in the grocery cart of many populations internationally, including China, Brazil, and the USA. Pineapple occupies an important place in the tropical agricultural cash crop market, being the third most important tropical fruit after bananas and mangoes [14,15]. O'Brien et al. (1970) [16] proposed an automated pineapple harvester that caused acceptable mechanical damage by using a ripening chemical that

enabled the machine to recover 99% of the fruit. Their harvester applied lateral and downward forces on the fruit while simultaneously applying an opposing force on the pedicel. The action resulted in a bending moment on the pedicel. A few researchers have studied pineapple identification, positioning [17–19] and picking end-effectors [20,21]. Research on the mechanization of pineapple harvesting, however, is still in its nascence [22,23]. In the past, studies on pineapple fruit plant detachment were focused on stalk cutting. Most results showed that the stalk cutting method can separate fruit from the plant easily, however, such methods have to locate the pineapple stalk accurately; this results in inefficiency.

The purpose of this paper is to study mechanized batch harvesting methods. A multi-flexible-fingered roller pineapple batch harvesting mechanism was designed according to pineapple's ellipsoidal shape and hard waxy peel. This harvesting device bends pineapple stalks and separates the fruit from the plant using two pairs of tilted flexible rubber fingers. Those fingers provide a breaking bending moment on the fruit, which simulates the process of manual picking. The moment required to break the abscission layer at the pineapple calyx was measured. The mechanics of the fingers acting on the pineapples were investigated, and the key parameters of a suitable harvesting mechanism were obtained.

2. Materials and Methods

2.1. The Physical and Mechanical Properties of Pineapples and Their Stems

Usually, both robotic and mechanical batch harvesting must ensure the lowest possible rate of damage to the fruit. The physical and mechanical properties of the fruit and stem define the basic premise for achieving damage-free harvesting.

2.1.1. Physical Characteristics of Pineapple Fruit and Plant

According to the United Nations Economic Commission for Europe (UNECE) standard for pineapples (FFV-49), the ripeness of pineapple can be classified into five stages from C0 to C4 depending on peel color: stage C0 contains 0% yellow, stage C1 0–25% yellow, stage C2 25–50% yellow, stage C3 50–75% yellow, and stage C4 75–100% yellow. Between C1 and C2 maturity, pineapples are easier to transport and less prone to damage [14]. The size and plant height of pineapples were measured (as shown in Figure 1) by using a random selection method in October 2021 in Shenwan Town, Zhongshan City, Guangdong Province, China (north latitude N22°18′18.46″; longitude E113°21′30.07″). Shenwan pineapples, also known as the Jinshan species, were transplanted to Shenwan in 1915 by repatriated Chinese who had been living in Peru. Two hundred pineapples with maturity stage C1 and C2 were selected to measure the maximum diameter (as shown in Figure 1a), length of fruit (as shown in Figure 1b) and the height of the plant. The samples selected were all pest-free and had reasonable planting gaps. At the measurement site, most of the pineapples were growing upright or leaning slightly. The statistical results are shown in Figure 2; the average and standard deviations are summarized in Table 1. The pineapple plant heights were relatively scattered, with the highest being 930 mm. Most of them were concentrated between 650 mm and 850 mm. The maximum diameter and length of the specimens were 142 mm and 152 mm, respectively. Most diameters and lengths were concentrated between 100–110 mm and 120–150 mm, respectively.

Table 1. Pineapple physical properties.

	Average Value/cm	Standard Error
Height of plant	70.56	9.19
Diameter	10.66	1.18
Length	13.23	0.59

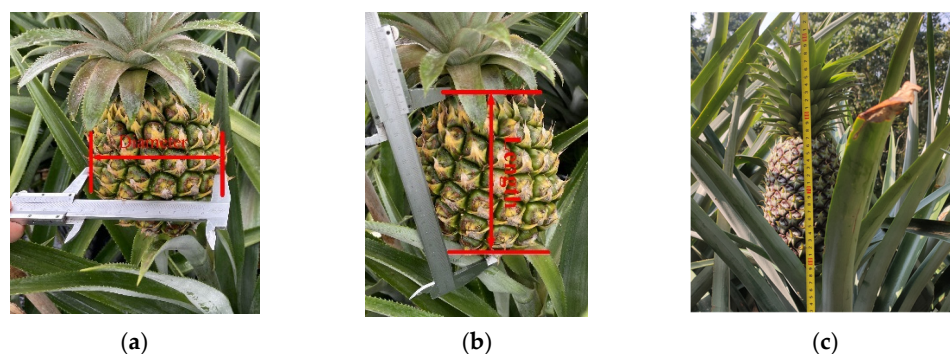


Figure 1. Measurement of pineapple physical property parameters. (a) Diameter of pineapple. (b) Length of pineapple. (c) Height of plant.

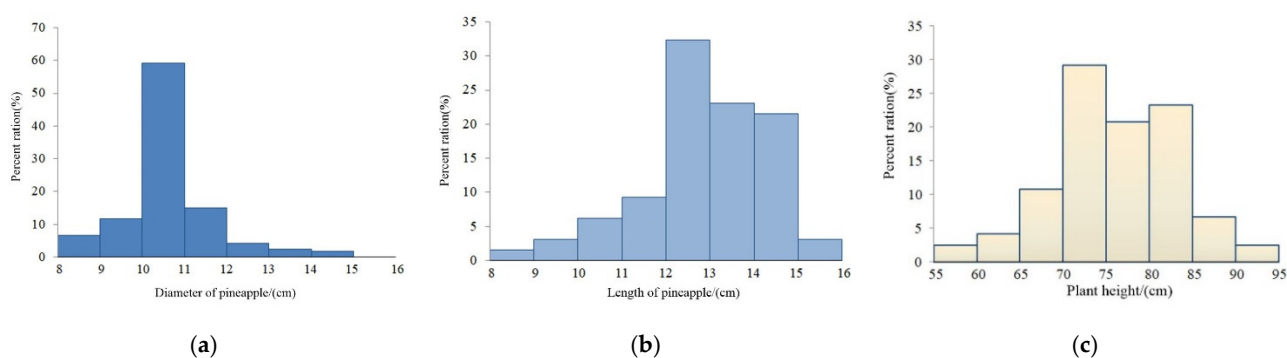


Figure 2. Histogram of statistical data. (a) Diameter of pineapple. (b) Length of pineapple. (c) Height of plant.

2.1.2. Pineapple Separation Mode from Plant

Fruit trees generally have four abscission zones [24], two for leaves and two for fruit. Fruits have two abscission zones: the first abscission zone is located between the branch and the fruit peduncle (AZ-A), and the second is found in the fruit calyx (AZ-C). Liu et al. (2008) [25] presented a detailed method measuring the bending and tensile strength of tomato fruit abscission layers (AZ-A). During their experiments, fruit stalks containing tomato abscission layers were placed on a miniature electronic universal testing machine. The bending moment required for the stalks to break at the abscission layer was calculated by force, displacement and the physical properties of the tomato fruit stalks. Liu et al. (2020) [26] derived a theoretical fracture model for the abscission layer at the pedicel of tomatoes under three different fruit plucking patterns (pulling, bending, twisting). The abscission zone at the pineapple calyx is also defined as AZ-C (as shown in Figure 3). The abscission layer is located in a zone of anatomically distinct cells. The presence of the abscission layer makes it easier for the fruit to separate from the plant.

Studies of hand-picking patterns provide greater insight into the optimal methods for separating the fruit from the plant [27]. In September 2021, we conducted a survey of pineapple hand-picking methods and concluded that there are two fruit plant detachment methods: the first method involves holding the pineapple with the left hand while the right hand cuts the stem with a knife, the second method involves holding the upper part of the pineapple with the right thumb and the lower part of the pineapple with the remaining fingers of the right hand and separating the pineapple from the plant by turning the hand to bend the abscission layer at the calyx.

The bending moment applied to the abscission layer at the calyx of the fruit enables the pineapple fruit to cleanly detach from the plant. Before we continue, the bending moment required to break the abscission layer at the calyx of the fruit needs to be measured. One hundred pineapple plants with maturity stages C1 and C2 were randomly selected from a pineapple plantation and wrapped in cling film to reduce the lateral force on the abscission

layer at the calyx of the fruit. Experiments were carried out within the room temperature range of 20–25 °C on one day and all fruits were labeled before the experiment.

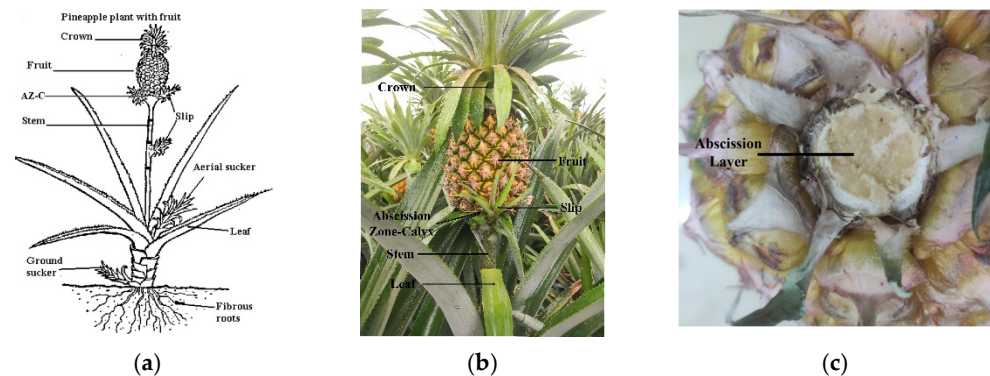


Figure 3. Schematic diagram of pineapple plant structure name. (a) Citrus leaf and fruit abscission zones. (b) Pineapple plant with fruit. (c) Pineapple abscission layer.

2.1.3. Mechanical Properties of the Abscission Layer at the Calyx of the Pineapple

All these experiments were carried out on a microcomputer-controlled electronic universal testing machine with an accuracy of $\pm 0.5\%$ and a resolution of $\pm 1/500,000$. The loading and unloading was controlled automatically by the microcomputer and data were recorded automatically. Before each experiment, fruits were divided into two groups: one with a maturity range of C1 and the other with a maturity range of C2. The pineapple plant was fixed horizontally on a jig and clamped without displacement in any direction. The stem was kept perpendicular to the inverted triangular indenter before the test. A force transducer with 250 N range was used to detect pressure. Loading rate for all tests was 0.33 mm/s. A test sample was shown in Figure 4a. The distance from the fracture end of each stem to the indentation position (at the blue line, as shown in Figure 4b) was measured separately. The length L' of the moment arm measuring method was demonstrated in Figure 4b. This measurement method can be simplified to a model shown in Figure 4c, where point A is the fruit calyx abscission layer and point B is the position of the stem under force. The bending moment required to break the abscission layer of the fruit calyx is calculated by peak force F' multiplied by L' . Some of the measured lengths L' were listed in Table 2.

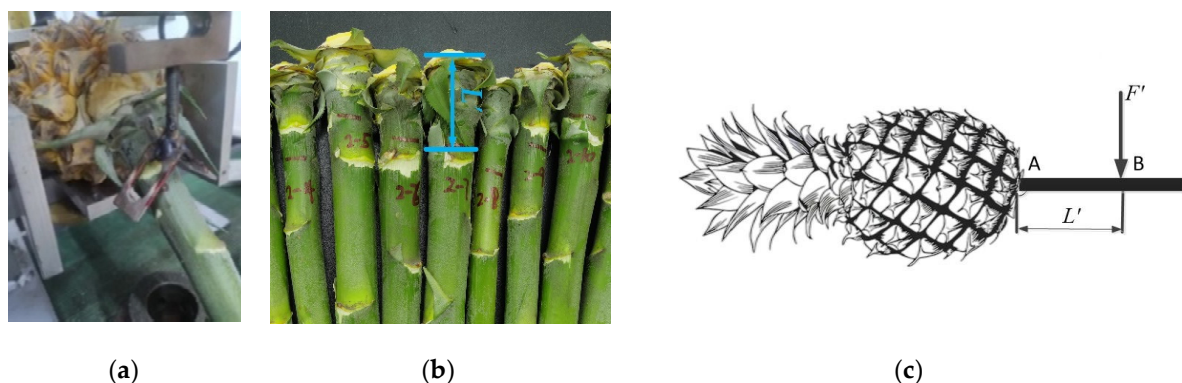


Figure 4. AZ-C layer of pineapple bending moment experiment. (a) Experimental process. (b) Moment Arm. (c) Simplified force diagram of the abscission layer bending test at the calyx of pineapple.

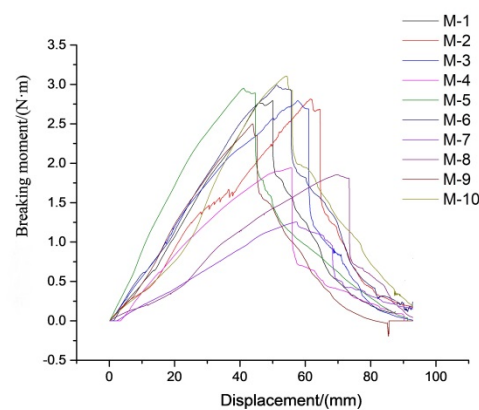
Table 2. Length.

Maturity Levels	L'1/mm	L'2/mm	L'3/mm	L'4/mm	L'5/mm	L'6/mm	L'7/mm	L'8/mm	L'9/mm	L'10/mm
C1	33	30	31	33	32	34	38	46	63	59
C2	36	43	51	47	37	35	45	42	37	60

2.1.4. Analysis of Experimental Results

Fruit stems were all broken from the abscission layer at the calyx of the fruit, and the required bending moment M was derived from Equation (1). Several test result diagrams of maturity C1 and C2 samples are shown in Figure 5, where the peak of each curve in the figure is the bending moment when the abscission layer at the calyx of the fruit breaks. The average and maximum bending moments with maturity levels C1 and C2 are shown in Table 3. The average and the maximum bending moments in stage C1 are greater than in stage C2.

$$M = F'L' \quad (1)$$

**Figure 5.** C2 group of bending moments.**Table 3.** Bending moment.

Maturity Levels	Average Bending Moment/(N·m)	Maximum Bending Moment/(N·m)
C1	3.67	4.96
C2	2.41	3.02

2.2. Pineapple Batch Harvesting Mechanism Design

2.2.1. Multi-Flexible-Fingered Roller Pineapple Harvesting Mechanism

The multi-flexible-fingered roller pineapple harvesting mechanism is shown in Figure 6. Flexible materials, such as rubber and plastic, have been widely used in various flexible clamps due to their super-elasticity and shock-absorbing properties (Navas et al., 2021) [4]. The flexible fingers made of super-elastic flexible material reduce damage to the fruit.

The harvesting device was taken out for analysis. It consists of three main parts: the flexible-fingered rollers, the leaf press shelf, and the frame. The rollers are arranged symmetrically on the frame and each roller is fitted with two rows of symmetrical flexible fingers, which rotate in opposite directions at the same angular speed to provide the bending moment. The radius R of the rollers is 55 mm and their thickness is 5 mm. The distance between the centers of the two rollers is 400 mm, according to the measured pineapple diameter (as shown in Table 1).

The schematic diagram of this operational method is shown in Figure 7. At the beginning of the harvesting process, the two rollers are inclined relative to each other, and the flexible fingers are oriented perpendicular to the ground. Then, the leaf press shelf is

pressed into the plant, plant leaves are pressed down to the ground, and the pineapple will be located in the middle of the two rollers. The rollers rotate in reverse at the same angular speed. The left flexible fingers touch the pineapple and push the plant to the right under the force from the left side. The right flexible fingers touch the pineapple and apply an opposing right side force on the fruit. Those flexible fingers together pluck the pineapple by applying a bending moment on the two sides of the pineapple. Then, fruit calyx at the abscission layer breaks off.

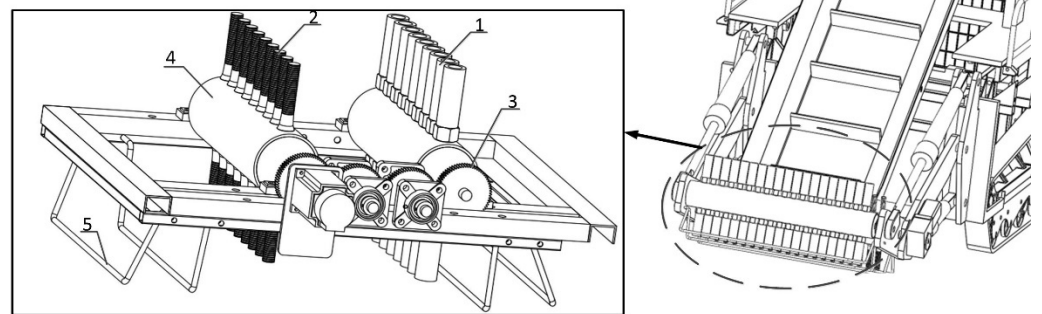


Figure 6. Multi-flexible-fingered roller of pineapple harvester. 1. Right flexible finger 2. Left flexible finger 3. Gear 4. Roller 5. Leaf press shelf.

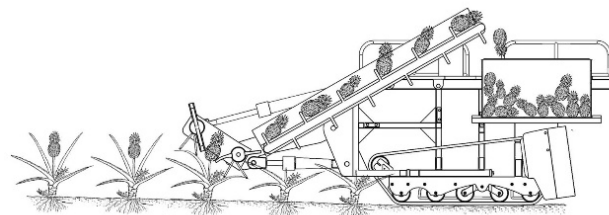


Figure 7. Schematic diagram of pineapple harvest.

2.2.2. Flexible Fingers Design and Force Deformation Analysis

To ensure sufficient space between the flexible finger and the pineapple and to protect the pineapple from damage, the left finger is designed as a solid circular cross-section flexible rod and is made of natural rubber (as shown in Figure 8). In Figure 8, N_i denotes the pressure of continuous bending unit i , length $L_0 = 120$ mm and diameter $\phi_1 = 22$ mm. Natural rubber has excellent resilience, plasticity and wear resistance, and is a common material for flexible picking devices [28].

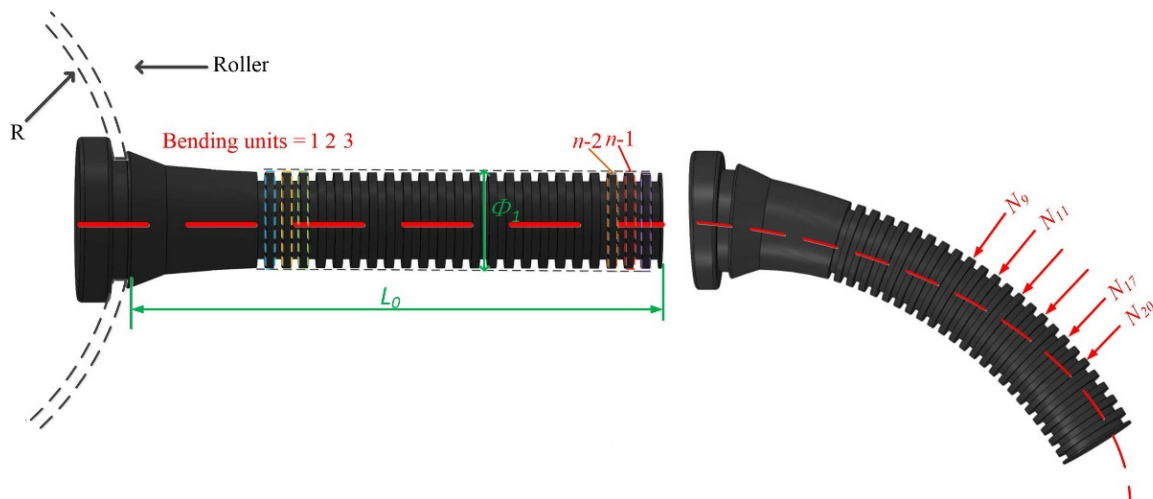


Figure 8. Left flexible finger.

The right flexible finger is designed as a nylon screw wrapped in hollow circular section silicone rubber tubing, as shown in Figure 9. In Figure 9, F_i denotes force i dispersed across the contact surface, $L_1 = 150$ mm, $\phi_2 = 16$ mm, $\phi_3 = 36$ mm and $L_2 = 120$ mm. The right flexible finger is fixed to the roller by two nuts. The nylon screw has strength, stiffness and high impact absorption capacity. This structure can reduce the sudden impact force of the flexible rod acting on the surface of the pineapple. In order to prevent relative slippage between the left flexible fingers and the pineapple and to increase the coefficient of friction on the contact surface, the surface of left flexible fingers is textured by bulges. The uneven surface of the pineapple engages with the bulges and generates greater friction.

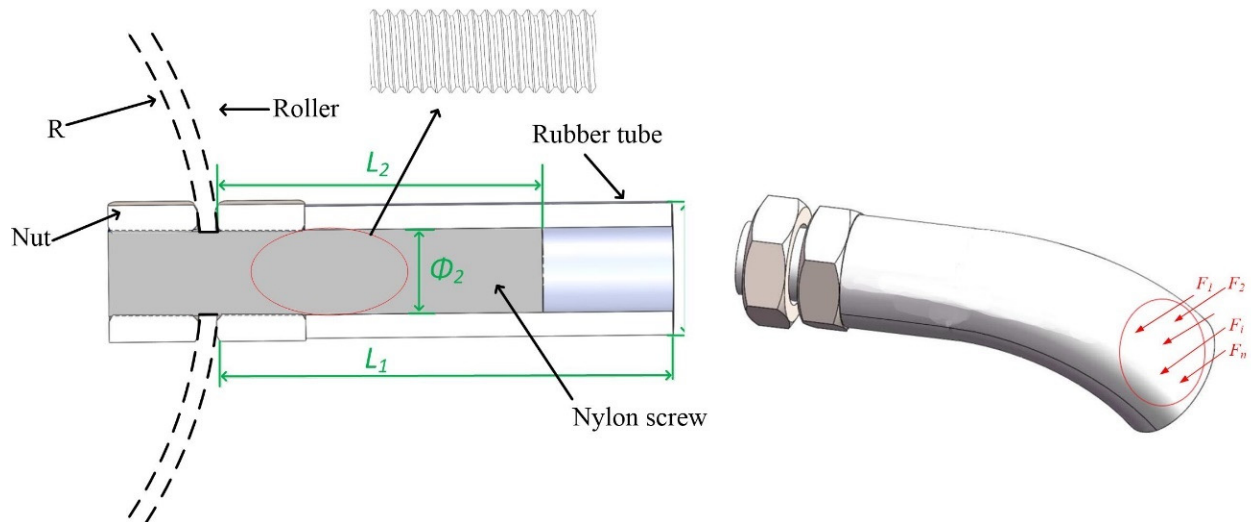


Figure 9. Right flexible finger.

The contact length between the left flexible finger and the pineapple must be sufficient, such that the force is spread over each small bending unit, and reaction force F_i on the pineapple surface can spread over the contact area. If the squeezed circular cross-section changes to an elliptical cross-section, the contact area between the surface of pineapple fruit and the flattened silicone rubber tube becomes larger, which also helps prevent damage to the fruits.

The structure of the flexible finger is assumed to be exact and regular in deriving its mechanical model. Rubber has large deformation and super elastic ability. It is difficult to construct a satisfactory and uniform model to express all of rubber's non-linear viscoelastic and stress-softening properties. The deformation that occurs when the rubber flexible fingers come into contact with the pineapple can be equated as a force deformation model for the flexible rubber cantilever beam that is fixed to the roller. Howell et al. (2001) [29] applied the pseudo-rigid body approach to analyze flexible beams and proposed a force deformation model to express large deformations of compliant cantilever beams. The compliant cantilever beam structure (as shown in Figure 10) with the force at the free end is equivalent to a rigid rod that is hinged together, and a torsion spring is added at the joint to analyze the trajectory of the end of the cantilever beam. The model of such a compliant cantilever beam is expressed as Equations (2)–(9).

$$I = \frac{\pi r^4}{4} \quad (2)$$

$$K = \frac{\gamma K_\theta EI}{l} \quad (3)$$

$$n = -\frac{1}{\tan \phi} \quad (4)$$

$$\eta = \sqrt{1 + n^2} \tag{5}$$

$$\theta' = \arcsin \frac{l_y}{\gamma l} \tag{6}$$

$$P = \frac{K\theta'}{\eta \gamma l \sin(\frac{\pi}{2} - \theta)} \tag{7}$$

$$\theta_0 = c_\theta \theta' \tag{8}$$

$$F = \eta P \tag{9}$$

where, I , K , θ' , θ_0 and F , ϕ are the moment of inertia of the circular section (m^4), the torsion spring constant, the pseudo-rigid-body angle ($^\circ$), the actual angle of rotation at the end of the flexible beam ($^\circ$), the load applied to the beam (N), and the angle of force F ($^\circ$), respectively; r is the circular section radius of the flexible finger (m); K_θ is the stiffness coefficient; γ is the characteristic radius factor; γl is the characteristic radius (m); E is Young's modulus of the material (MPa); K_θ , γ are constants that can be derived by checking the table.

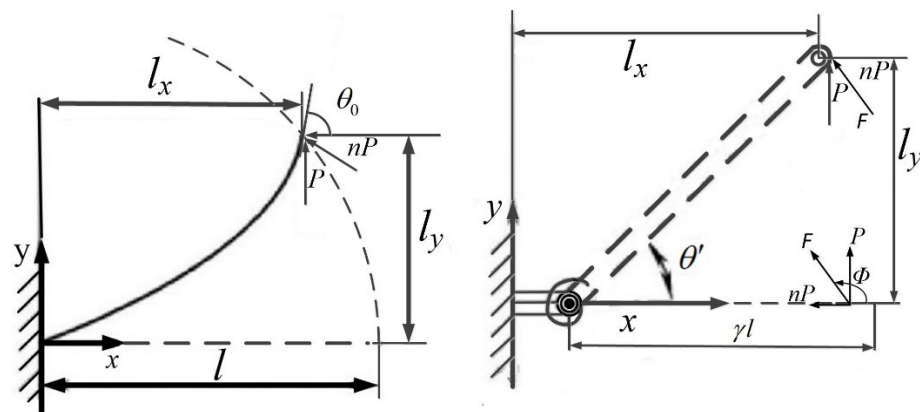


Figure 10. Pseudo-rigid-body model.

When the Shore hardness A of rubber is between 20 and 80, the Young's modulus E of rubber can be approximated by the Shore hardness A [30], and is expressed as Equation (10).

$$\log E = 0.0235S - 0.6403 \tag{10}$$

where S is Shore A hardness, (HA).

The Shore hardness A of the rubber flexible finger was measured by a SYNTEK digital Shore hardness A tester. This was measured by pressing the pressure needle vertically into the plane of the rubber flexible finger specimen; the needle and the specimen were held in full contact for 1 s to stabilize the value and then record the data. Five positions were randomly selected as measuring points, and their average was taken as the final Shore hardness A . The measured Shore hardness A of the rubber flexible finger was 54.5. Radius r , length l , and length factor γ were 11 mm, 96 mm and 0.85, respectively. Therefore, the Young's modulus of the flexible finger rubber is 4.375. The relationship between l_y and F was derived according to Equations (6), (7) and (9).

In order to verify that the theoretical model was also applicable to the flexible fingers of circular cross-section, one end of a flexible finger was fixed on a clamp, a load perpendicular to the center line of the flexible finger was applied at the other end ($l = 96$ mm). Because the load was perpendicular to the center line of the sample, n was equal to 0. The experiment was carried out on a micro-controlled electronic universal testing machine with a loading speed of 0.4 mm/s and the data were automatically recorded by a microcomputer. Each recorded displacement was taken as l_y and substituted into the Equation (6) to calculate θ' and further calculate theoretical force F . The displacement force curve of the theoretical

force F and the measured force are both plotted on the same coordinates, as shown in Figure 11. The recorded and calculated displacement-force curves are very similar. This result indicates that the flexible rubber cantilever beam can be characterized by the pseudo-rigid-body method.

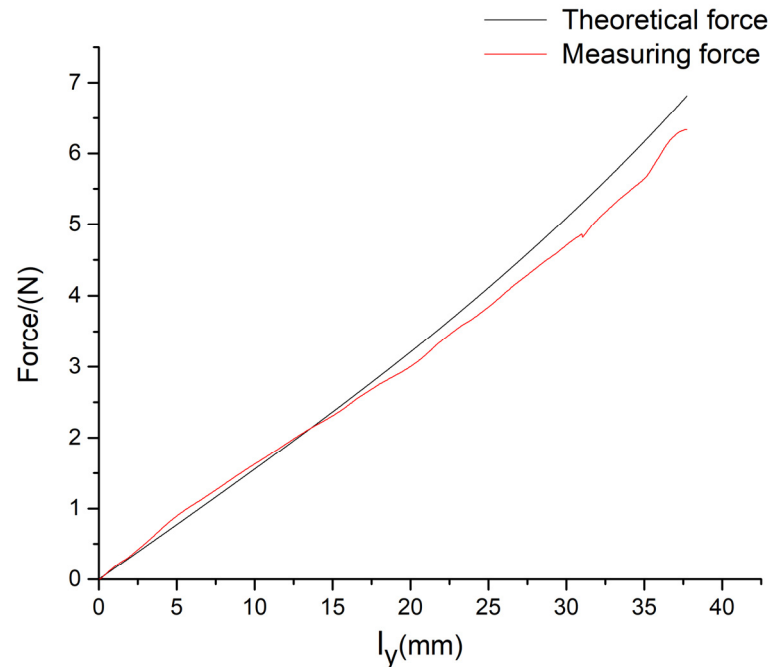


Figure 11. Displacement—force.

2.2.3. Mechanical Analysis of the Critical Fracture State of the Abscission Layer under the Action of a Flexible Finger

The geometry of the pineapple can be approximated as an ellipsoidal shape (Bhat et al., 2020). We will approximate the central vertical profile of the pineapple as an ellipse. The maximum diameter and the length of pineapple were taken as the short and long axis of the ellipse, respectively. The harvesting model was simplified to the structure shown in Figure 12. The connection between the pineapple stalk and the ground was simplified as a hinge and the pineapple stalk was considered as a rigid body. According to Equations (6) and (7), the shorter the distance between the force applied to the flexible finger to the fixed end, the greater the force required and deform the flexible finger to the same angle. The distance between the end of the nylon screw and the end of the finger was 30 mm. Because the right finger is significantly more rigid than the left finger, it was taken to be a rigid body. The kinematic mechanism was analyzed according to the above approximations. Both rollers rotated in reverse at the same angular speed, the left flexible finger touched the pineapple fruit first and the whole pineapple plant rotated around the fixed hinge point as shown in Figure 12a. Then, the end of the right flexible finger contacted the pineapple fruit and pushed the pineapple fruit backwards. Finally, the abscission layer at the calyx of the pineapple broke under the action of the two flexible fingers, as shown in Figure 12b. The contact process between the flexible fingers and the pineapple fruit is complex. The only problem that needs to be solved is how to keep the bending moment of the two fingers greater than that broken bending moment of the abscission layer. Therefore, the position of each contact point at the critical breaking state needs to be analyzed.

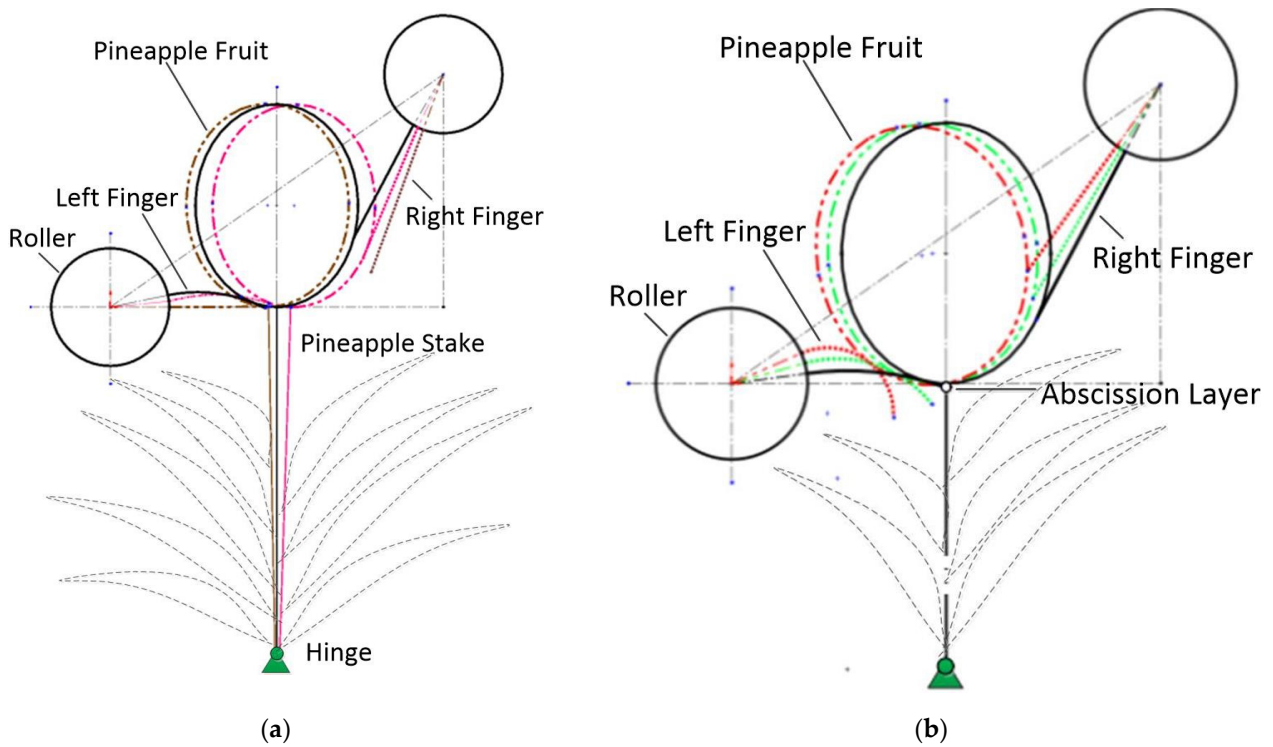


Figure 12. Schematic diagram of the interaction of flexible fingers with pineapple. (a) Before the right finger contact. (b) After the right finger contact.

A coordinate system was established, as shown in Figure 13. Its origin is located at the center of the left roller. Assuming that the initial position of the pineapple was at the center of both rollers in the x -axis direction and that the y -axis direction was unfixed, the coordinates of the left roller center O_1 and the right roller center O_2 were set as (x_1, y_1) and (x_2, y_2) , respectively. The lower vertex C of the long axis of pineapple fruit was set as (x_c, y_c) . θ is the relative tilt angle of the two rollers. θ_1 is the angle between the flexible finger and the line O_1O_2 .

$$x_2 = x_1 + L \cos \theta \tag{11}$$

$$y_2 = y_1 + L \sin \theta \tag{12}$$

$$x_c = \frac{L \cos \theta}{2} \tag{13}$$

$$\theta_1 = \theta_2 \tag{14}$$

where L is the distance between the centers of the two rollers.

The tangent line of the ellipse is expressed as Equation (15). The ellipse in the coordinate system is expressed as Equation (16).

$$\frac{\xi}{a^2} + \frac{\psi}{b^2} = 1 \tag{15}$$

$$\frac{(y - a - y_c)^2}{a^2} + \frac{(x - 0.5L \cos \theta)^2}{b^2} = 1 \tag{16}$$

where, a and b is the long and short semi-axes of the ellipse. The expressions of ξ and ψ are as follows:

$$\xi = (v - a - y_c)(L \sin \theta - a - y_c) \tag{17}$$

$$\psi = (\partial - 0.5L \cos \theta)(L \cos \theta - 0.5L \cos \theta) \tag{18}$$

where (∂, v) is a point on the ellipse.

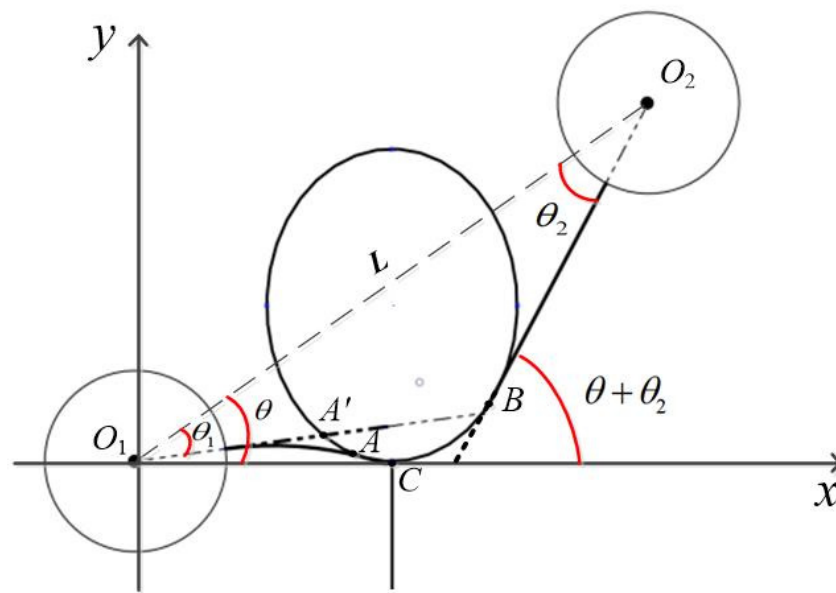


Figure 13. Multi-flexible fingers harvesting model of pineapple.

Substituting point $B(x_b, y_b)$ into (x, y) in Equation (16) and (∂, v) in Equations (17) and (18), and point $O_2(x_2, y_2)$ into (x, y) in Equations (17) and (18), the contact position x_b, y_b between the right flexible finger and the pineapple can be calculated and expressed as $x_b = f_1(\theta, y_c)$ and $y_b = f_2(\theta, y_c)$, where $x_b > 0$.

The relationship between θ and θ_2 can be derived from Equations (19), (20) and their geometric relationship can be expressed as $\theta_2 = f_3(\theta, y_c)$. The slope of the line $O_2-B \frac{dy}{dx}$ is as follows:

$$\frac{dy}{dx} = \frac{y_2 - y_b}{x_2 - x_b} \tag{19}$$

and

$$\frac{dy}{dx} = \tan(\theta + \theta_2) \tag{20}$$

The coordinates of the intersection $A'(x_a', y_a')$ in Figure 13 were calculated using Equations (16), (21) and expressed as $x_a' = f_4(\theta, y_c), y_a' = f_5(\theta, y_c)$.

$$y_a' = \tan(\theta - \theta_1)x_a' \tag{21}$$

where $x_a \geq 0$.

Figure 14 shows a diagram of the state of the left flexible finger under force. Take point $A(x_a, y_a)$ as the final intersection of the deformed flexible finger with the ellipse (fruit contour). The horizontal coordinate of point $A x_a$ can be computed approximately using Equation (22). Its vertical coordinate y_a was calculated by substituting x_a into the elliptic Equation (16). Symbol d represents the magnitude of the flexible finger's longitudinal deformation, and its solution formula is shown in Equation (23). The inclination angle θ_A of the tangent line of ellipse at point A was calculated by substituting the coordinates of point A into the ellipse tangent line Equation (15) and expressed as $\theta_A = f_6(\theta, y_c)$. The action angle ϕ of the flexible finger can be deduced by the geometric relationship in Figure 14, as in Equation (24).

$$x_a = \frac{x_a' + x_c}{2} \tag{22}$$

$$d = \frac{|y_a - \tan(\theta - \theta_1)x_a|}{\sqrt{1 + (\tan(\theta - \theta_1))^2}} \tag{23}$$

$$\phi = \theta_A + \theta - \theta_1 + \frac{\pi}{2} \tag{24}$$

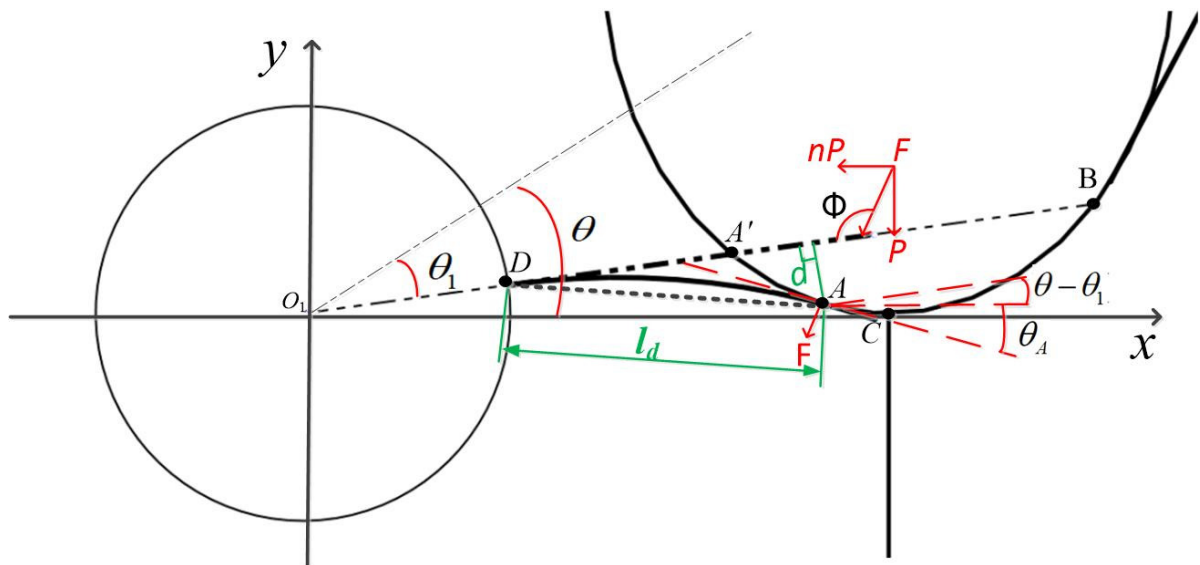


Figure 14. Forced state of the left flexible finger.

Equation (25) is the function of Circle O_1 . The coordinates of intersection point D (x_d, y_d) between line O_1A' and circle O_1 are computed by Equations (25) and (26). Symbol l_d denotes the distance between the point A and point D , and its computing formula is Equation (27).

$$x_d^2 + y_d^2 = R^2 \tag{25}$$

$$y_d = \tan(\theta - \theta_1)x_d \tag{26}$$

$$l_d = \sqrt{(x_a - x_d)^2 + (y_a - y_d)^2} \tag{27}$$

where R is the radius of the roller.

The left flexible finger will deform after it makes contact with the pineapple fruit. Its deformation displacement can also be seen as an offset pushed by force F . According to the flexible finger model in Section 2.2.2, the relationship among parameters l_y , d , γl , and l_d satisfy Equations (28) and (29).

$$l_y = d \tag{28}$$

$$\gamma l = l_d \tag{29}$$

Then, input parameters $r = 11$ mm, $\gamma = 0.85$, $K_\theta = 2.65$ and $S = 53.5$ HA, $E = 4.375$ MPa into Equations (2)–(9) together, resulting in the function of force $F = g(\theta, y_c)$.

Figure 15 shows a schematic representation of the forces on the pineapple when it is separated from the plant. Friction between the pineapple fruit surface and finger can be ignored, because the bending moment created by them is very small. Therefore, bending moment M is co-generated by F_A and F_B , $M = M_1 + M_2$. Moment M_1 and M_2 can be deduced according to Figures 14 and 15 and the geometrical relations. M_1 and M_2 are expressed as Equations (30) and (31), respectively.

$$M_1 = F_A[-\cos\theta_A|0.5L\cos\theta - x_a| - \sin\theta_A|y_a - y_c|] \tag{30}$$

$$M_2 = F_B[\cos(\theta_2 + \theta)|x_b - 0.5L\cos\theta| + \sin(\theta_2 + \theta)|y_b - y_c|] \tag{31}$$

F and F_A are equivalent reaction forces, so that

$$F = F_A \tag{32}$$

Parameters x_b, y_b, x_a, y_a and F_A are all functions of the independent variables (θ, y_c) . Therefore, the sum of the bending moment can be expressed by Equation (33).

$$M = M_1 + M_2 = f(\theta, y_c, F_B) \tag{33}$$

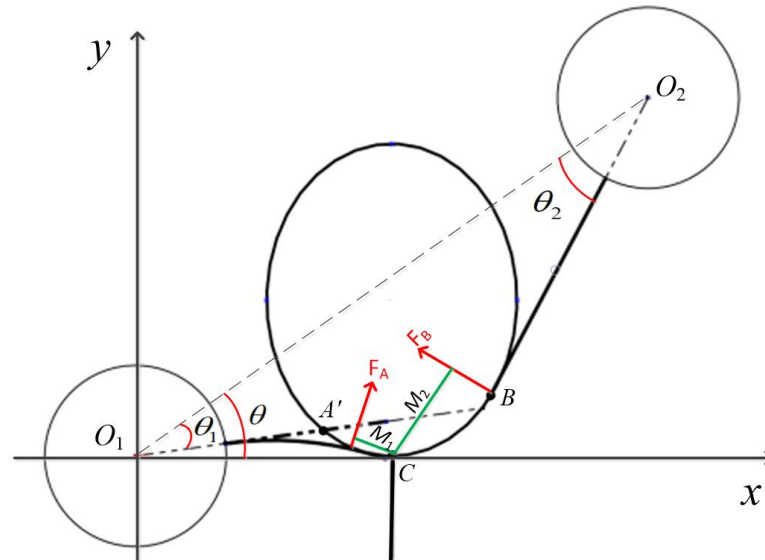


Figure 15. Force diagram of pineapple under the double flexible fingers.

2.2.4. Key Parameters of the Harvesting Mechanism

A load of 50 N cannot cause damage to the pineapple fruit [31]. Therefore, the maximum interaction force between each finger and the pineapple fruit should be less than 50 N, meaning if F_A and F_B reach 50 N, the bending moment formed by the two flexible fingers must be greater than the moment required to break the abscission layer at the calyx of the pineapple. The force F_A , generated by the left flexible finger on the pineapple, is a function of θ and y_c . A constraint as expressed in Equation (34) can be derived to avoid injuring the fruit.

$$M = M_1 + M_2 = f(\theta, y_c, 50) \geq M_{ac} \tag{34}$$

where M_{ac} is the actual measured moment required to break the abscission layer at the pineapple calyx (as shown in Table 3).

Another prerequisite for successful harvesting is that the fruit itself can be fed into the cavity between the two rollers; the horizontal distance between the two rollers at a certain inclination angle must satisfy Equation (35). According to this constraint, inclination angle θ must be less than 57° .

$$(L \cos \theta - 2R) > 2b \tag{35}$$

A program was designed using MATLAB R2020a (The Mathworks Inc., Natick, MA, USA) software to calculate M under the different y_c . The range of θ is $[0, 57^\circ]$. Due to the possible relative position of the pineapple fruit and the harvesting device (in the vertical direction), the range of y_c is $[-30 \text{ mm}, 20 \text{ mm}]$. The traversal interval of θ and y_c were set as 1° and 1 mm, respectively. The computed space M is shown in Figure 16.

Figure 16 shows that, regardless of y_c , bending moment M increases with θ . If the angle θ does not change, the y_c gets bigger, and the bending moment becomes smaller. When θ is 51° and y_c is -30 mm , the bending moment reached the maximum. The maximum bending moment created by the pair of flexible fingers is 2.5 N·m. The force F_A applied to the pineapple by the left flexible finger at different positions y_c was calculated according to the pseudo-rigid-body model under conditions of θ being equal to $0^\circ, 35^\circ$ and 40° , and was plotted in Figure 17. Figure 18 shows the bending moment under conditions of θ being equal to $0^\circ, 35^\circ$ and 40° . It is clear from Figure 17 that F_A is less than 50 N and will not damage fruit. It can be observed in Figure 18 that, when the inclination angle θ is

35° and 40°, the bending moment provided by the pair of flexible fingers is larger than 2 N·m. According to the above calculations, and in keeping with the design principle of compactness, the final inclination angle θ is set as 35°. In the process of harvesting, the harvesting possibility area of y_c is controlled within [−30 mm, 20 mm].

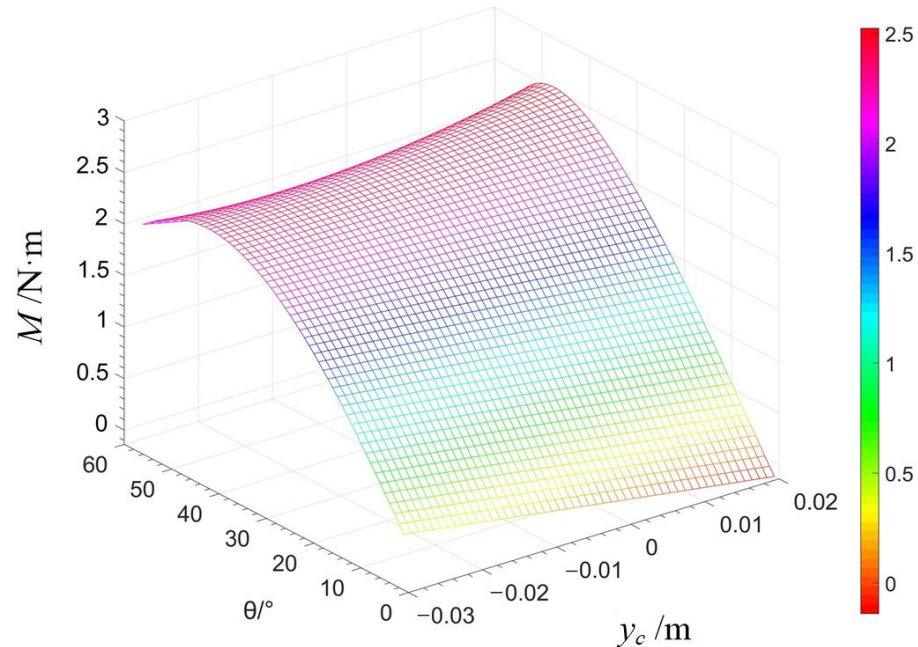


Figure 16. Bending moment M .

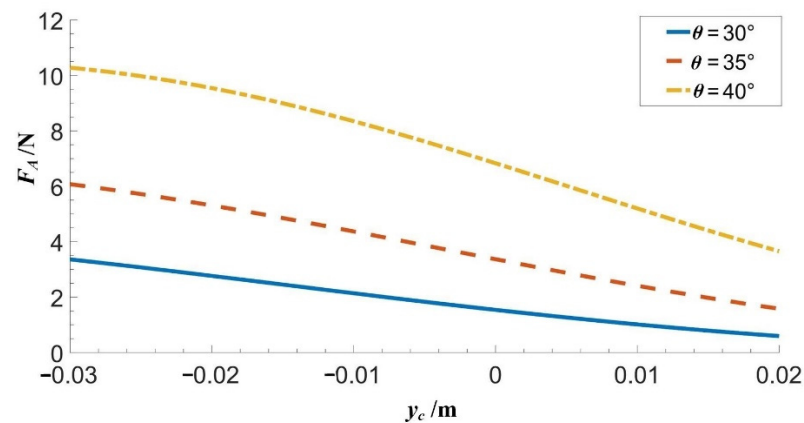


Figure 17. Force F_A on the left flexible finger at 30°, 35° and 40°.

Because the maximum bending moment required to separate the pineapple from the plant is 4.96 N·m (as listed in Table 3), at least two pairs of flexible fingers must be in contact with the pineapple to provide a sufficient bending moment. Therefore, the distance between the two flexible fingers should be less than the diameter of the fruit. The constraint formula is as shown in Equation (36).

$$L_f \leq 2nb \quad (36)$$

where L_f is the distance between the two flexible fingers; n is a safety coefficient, $0 < n < 1$. The gaps between the two adjacent flexible fingers on the left and right rollers were set as 30 mm and 10 mm, respectively.

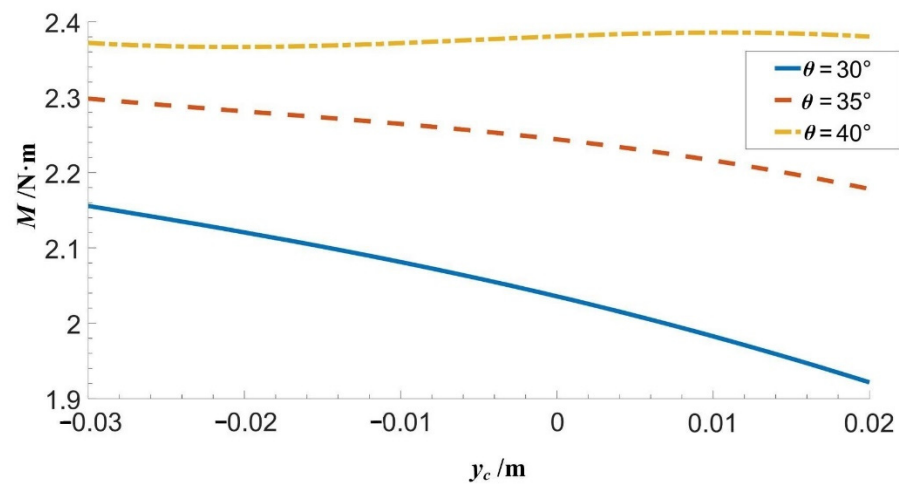


Figure 18. Bending moment M at 30° , 35° and 40° .

2.3. Experiment Method

According to the results calculated in Section 2.2, the main parameters of the pineapple harvesting mechanism: the diameter of the roller is 110 mm; the inclination angle of the two rollers is 35° ; the relative distance between the two rollers is 400 mm; the length of the left flexible fingers equaling to 120 mm, the clearance between each of the left flexible fingers equaling to 30 mm, the length of the right flexible fingers equaling to 150 mm, and the clearance between each of the right flexible fingers equaling to 10 mm.

The experimental pineapple harvesting machine is shown in Figure 19. In the harvesting experiment, the rollers rotated at the same speed. During the rapid grasping of fruit by two fingers, the peak collision force had a positive correlation with the collision speed, and the collision time was negatively correlated with the collision speed [32]. The speed of the roller was set to 100 r/min in order to prevent damage to the fruit caused by collision force. In order to further clarify the actual state of contact between the pineapple and the flexible fingers, the experiment was recorded with a camera.

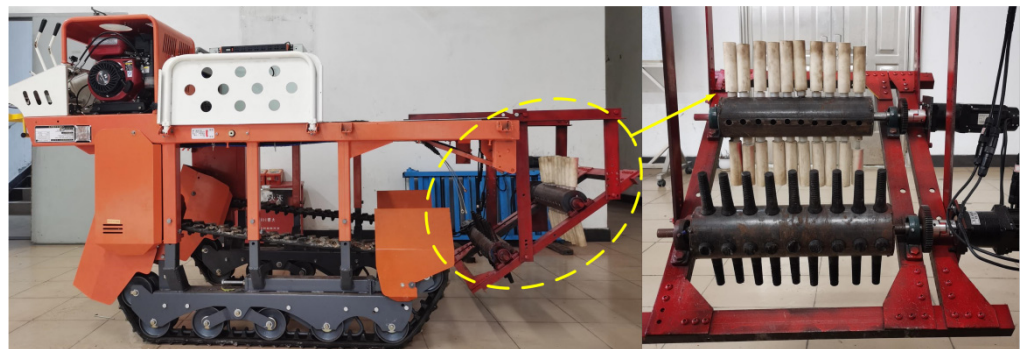


Figure 19. Pineapple harvesting testing machine.

A case of the harvesting process in laboratory is shown in Figure 20. 400 samples, with 90–120 mm diameters, 100–140 mm lengths and ripeness stages between C1 and C2 were selected to do this trial in the laboratory. Before the trial, the bottom of the pineapple stalk was fixed and was randomly placed in different positions within the harvesting possibility zone. Possible damage areas were marked with a note pen before the test. Because the pineapple has a hard waxy peel, most damage occurred in the pulp. It was hard to find inside damage with upon first glance. The detached fruits were stored in a temperate box at 20°C for three days, and then cut open in the possible damaged areas to check for injury. In order to further evaluate the harvesting performance of the multi-flexible-fingered roller

in the natural environment, 80 samples were used to do trial in natural environment, as shown in Figure 21.

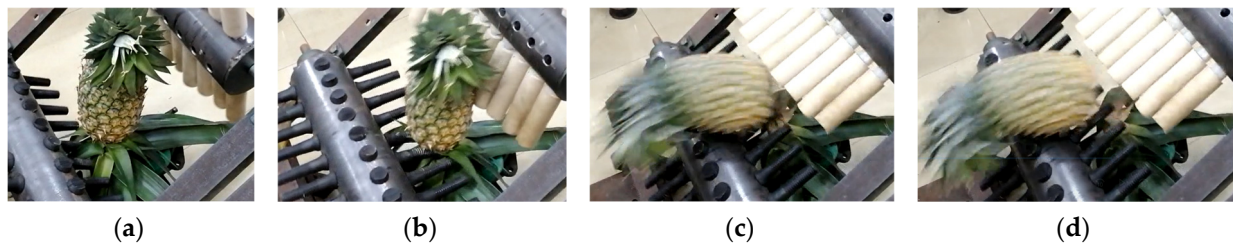


Figure 20. Some pictures of pineapple harvesting in a harvesting process. (a) Pineapple was located in the harvesting possibility area. (b) Left fingers contacted the pineapple. (c) Abscission layer was broken. (d) Pineapple fruit was detached from the plant.



Figure 21. Some pictures of pineapple harvesting in natural environment.

To evaluate the performance of the proposed mechanism harvesting pineapple fruit, three metrics were defined. The first metrics was the harvesting rate expressed in Equation (37). The harvesting rate is the number of intact harvested pineapple fruits per total harvested pineapple fruits. The second metric was the damage rate expressed in Equation (38). The damage rate is the number of injured pineapple fruits per total harvested pineapple fruits. In this study, the fruit had to be completely intact. Cases of small damage (diameter less than 10 mm) were counted as 60% damaged and cases of larger damage were counted as totally damaged. Both types of damage were considered harvesting failures. The third metric was harvesting speed expressed in Equation (39).

$$\text{Harvesting rate} = \frac{\text{Intact harvested fruits number}}{\text{Total fruits number}} \times 100\% \quad (37)$$

$$\text{Damage rate} = \frac{\text{Injured fruit number}}{\text{Intact harvested fruits number}} \times 100\% \quad (38)$$

$$\text{Harvestingspeed} = \frac{\text{Harversted fruitnumber}}{\text{Time}} \quad (39)$$

3. Results and Discussion

In the laboratory trial, the rate of successful harvest was 85%, with 5% damaged. The harvesting experiment using the multi-flexible-fingered roller of pineapple harvester was conducted in the natural environment, which is shown in Figure 21. The results, in the natural environment, showed harvesting rate and damage rate to be 78% and 8% respectively. The harvesting speed was about 1 s per fruit. When the roller is long enough,

multiple pineapples can be harvested in a single harvesting process. Most successfully harvested pineapples were separated from the plant at the calyx by the action of the flexible finger, with a small amount separating from the plant due to the breakage of the stem nodes. There were four factors that likely led to the majority of harvest failure. The first was that the flexible finger is too short for small fruits or too long for big fruits. The second was that the gaps between the two adjacent flexible fingers are too big for small fruits, allowing only one pair of flexible fingers to act on the surface of the fruit. A single pair of flexible fingers cannot provide a sufficient bending moment to separate fruit from the plant. The third factor was that the tilt angle of some pineapple stalks was greater than 30° and could not be fed into the cavity between the two rollers. The fourth possibility was that the harvesting position is too high to form the bending moment, and the force on the fruit only acted to pull the pineapples fruit away from the plant. The force direction of the left and right flexible fingers acting on a few of the fruits tended to be parallel and formed a squeezing force. Such squeezing force is the main cause of damage.

The end-effector designed by Du et al. (2019) [31] achieved a fruit damage rate of 5%, a plant damage rate of 0%, a fruit fall rate of 1.7% and an average picking speed of 14.9 s per fruit. An automatic pineapple picking and collecting straddle machine proposed by Guo et al. (2021) [33] reached 1636 plants/hour by simulation. A robotic system for harvesting pineapples developed by Nguyen et al. (2020) [34] can pick 95.55% fruit with a speed of 12 s per fruit. FU et al. (2020) [35] designed a semi-automatic screw-type pineapple picking–collecting machine and achieved a picking speed of 17.99 s per plant. Ma et al. (2020) [36] designed a pineapple picking manipulator and reached a picking rate of 80%, with an average picking time 13.5 s. Their harvesting rates vary from 80% to 95%, and their damage rates vary from 0% to 5%. However, the average picking speed of their methods was slower than 14 s/fruit. Besides, those robotic fruit picking methods require precise positioning pineapple. Comparatively, our multi-flexible-fingered roller pineapple harvesting method is faster, with no requirement of precise positioning.

4. Conclusions

A mechanized pineapple harvesting mechanism was put forward by simulating the process of manual harvest. In the presented solution, the broken bending moments of the pineapple abscission layer were measured by a universal electronic testing machine, and the results showed that the maximum bending moment to break the abscission layer at the calyx of the pineapple was 4.96 N·m. The experimental curve is very similar with the curve obtained from the pseudo-rigid-body theory, which indicated that the pseudo rigid body theory can be used to analyze the large deformation of flexible fingers. The key parameters of the harvesting mechanism were as follows: the rollers should be inclined at 35° , the left flexible fingers should be 120 mm long, the gap between each of the left flexible fingers should be 30 mm, the length of the right flexible fingers should be 150 mm long, and the gap between each of the right flexible fingers should be 10 mm.

An experimental device was developed for trial. Experimental results showed that most of the pineapple fruits could be successfully harvested. The successful harvesting rate was 85% with a damage rate of 5% in laboratory; in natural environment, harvesting rate and damage rate were 78% and 8%, respectively. The harvesting speed was about 1 s per fruit. When the pineapples were located in the harvesting possibility area, the harvesting mechanism can harvest most of the pineapples with a diameter of 90–120 mm and a length of 110–150 mm. According to above results, the machinery can sufficiently meet the usage demand of pineapple harvesting and be more efficient. For unsuccessful harvesting, the failure resulted from mismatched flexible finger length, fruit size and harvesting posture and position. A small fruit diameter probably leads to insufficient contact between the flexible finger and the pineapple, and an insufficient bending moment. If the harvesting position is too high, the contact position between the two flexible fingers and the pineapple is almost at the same horizontal height, and the bending moment cannot be formed. The

harvest damage mainly resulted from the excessive size of some of the fruits, where an excessive extrusion force formed when the fingers interacted with the pineapple fruit.

The limitations of current research are that the inclination angle between the two rollers cannot be adjusted, and there is no automatic device to lift the harvesting mechanism. In future research, the hydraulic rod will be designed to adjust the inclination of the two rollers. The adaptability of the mechanism will also be improved.

Author Contributions: Conceptualization, T.Z. and W.L.; methodology, T.Z., W.L. and T.L.; investigation, Y.C. and J.Q.; data curation, Y.C., W.L. and Y.Z.; formal analysis, Y.Z. and J.Q.; writing—original draft, W.L.; writing—review and editing, W.L., T.L.; project administration, T.L.; funding acquisition, T.L. All authors have read and agreed to the published version of the manuscript.

Funding: This research was funded by the National Natural Science Foundation of China (grant no. 52175229).

Data Availability Statement: The data presented in this study are available on request from the corresponding author.

Conflicts of Interest: The authors declare no conflict of interest.

References

1. CIGR Handbook of Agricultural Engineering, Volume III Plant Production Engineering, Chapter 1 Machines for Crop Production, Parts 1.1.1–1.1.4 Human-Powered Tools and Machines. pp. 1–22. Available online: <https://elibrary.asabe.org/abstract.asp?aid=36337> (accessed on 1 May 2022).
2. Liu, T.H.; Ehsani, R.; Toudeshki, A.; Zou, X.J.; Wang, H.J. Experimental study of vibrational acceleration spread and comparison using three citrus canopy shaker shaking tines. *Shock. Vib.* **2017**, *2017*, 9827926. [[CrossRef](#)]
3. Kearsley M, W. Principles and practices for harvesting and handling fruits and nuts. *Food Chem.* **1984**, *14*, 234–235.
4. Navas, E.; Fernández, R.; Sepúlveda, D.; Armada, M.; Gonzalez-de-Santos, P. Soft grippers for automatic crop harvesting: A review. *Sensors* **2021**, *21*, 2689. [[CrossRef](#)] [[PubMed](#)]
5. Zhang, Z.; Igathinathane, C.; Li, J.; Cen, H.; Lu, Y.; Flores, P. Technology progress in mechanical harvest of fresh market apples. *Comput. Electron. Agric.* **2020**, *175*, 105606. [[CrossRef](#)]
6. Liu, J.; Li, Z.; Li, P. History and Present Situations of Robotic Harvesting Technology: A Review. In *Rapid Damage-Free Robotic Harvesting of Tomatoes*; Springer: Singapore, 2021; pp. 1–106.
7. Shi, Y.; Wang, Y.; Zhang, Z. Design, Test, and Improvement of a Low-Cost Fresh Market Apple Harvest-Assist Unit. In *Mechanical Harvest of Fresh Market Apples*; Springer: Singapore, 2022; pp. 23–37.
8. Roshanianfard, A.; Noguchi, N. Pumpkin harvesting robotic end-effector. *Comput. Electron. Agric.* **2020**, *174*, 105503. [[CrossRef](#)]
9. Sanders, K.F. Orange harvesting systems review. *Biosyst. Eng.* **2005**, *90*, 115–125. [[CrossRef](#)]
10. Jianqiao, W.U.; Shengzhe, F.A.N.; Liang, G.O.N.G.; Jin, Y.U.A.N.; Qiang, Z.H.O.U.; Chengliang, L.I.U. Research status and development direction of design and control technology of fruit and vegetable picking robot system. *Smart Agric.* **2020**, *2*, 17.
11. Jutras, P.J.; Coppock, G.E.; Patterson, J.M. Harvesting citrus fruit with an oscillating air blast. *Trans. ASAE* **1963**, *6*, 192–194.
12. Sessiz, A.; Özcan, M.T. Olive removal with pneumatic branch shaker and abscission chemical. *J. Food Eng.* **2006**, *76*, 148–153. [[CrossRef](#)]
13. Li, P.; Lee, S.H.; Hsu, H.Y. Review on fruit harvesting method for potential use of automatic fruit harvesting systems. *Procedia Eng.* **2011**, *23*, 351–366. [[CrossRef](#)]
14. Ikram, M.M.M.; Mizuno, R.; Putri, S.P.; Fukusaki, E. Comparative metabolomics and sensory evaluation of pineapple (*Ananas comosus*) reveal the importance of ripening stage compared to cultivar. *J. Biosci. Bioeng.* **2021**, *132*, 592–598. [[CrossRef](#)] [[PubMed](#)]
15. Bhat, K.; Chayalakshmi, C.L. Microcontroller-Based Semiautomated Pineapple Harvesting System. In *International Conference on Mobile Computing and Sustainable Informatics*; Springer: Cham, Switzerland, 2020; pp. 383–392.
16. O'Brien, M.; Kahl, W.H.; Moffett, L. Is mechanically harvesting pineapple practical? *Agric. Eng.* **1970**, *51*, 564–565.
17. Li, B.; Ning, W.; Wang, M.; Li, L. In-field pineapple recognition based on monocular vision. *Trans. Chin. Soc. Agric. Eng.* **2010**, *26*, 345–349. (In Chinese with English Abstract)
18. Dong-Jian, H.E.; Zhang, L.Z.; Xiang, L.I. Design of automatic pineapple harvesting machine based on binocular machine vision. *J. Anhui Agric. Sci.* **2019**, *47*, 207–210. (In Chinese with English Abstract)
19. Jiang, T.; Guo, A.F.; Cheng, X.B.; Zhang, D.; Jin, L.I. Structural design and analysis of pineapple automatic picking-collecting machine. *Chin. J. Eng. Des.* **2019**, *26*, 577–586. (In Chinese with English Abstract)
20. Kurbah, F.; Marwein, S.; Marngar, T.; Sarkar, B.K. Design and Development of the Pineapple Harvesting Robotic Gripper. In *Communication and Control for Robotic Systems*; Springer: Singapore, 2022; pp. 437–454.
21. Joy, P.P.; Rashida, R.T. *Harvesting and Post-Harvest Handling of Pineapple*; Pineapple Research Station (Kerala Agricultural University): Vazhakulam, India, 2016; pp. 686–710.
22. Goren, R. Anatomical, physiological, and hormonal aspects of abscission in citrus. *Hortic. Rev.* **2010**, *15*, 145–182.

23. Jizhan, L.; Pingping, L.; Zhiguo, L.; Hanping, M. Experimental study on mechanical properties of tomatoes for robotic harvesting. *Trans. Chin. Soc. Agric. Eng.* **2008**, *24*, 64–70.
24. Liu, J.; Peng, Y.; Faheem, M. Experimental and theoretical analysis of fruit plucking patterns for robotic tomato harvesting. *Comput. Electron. Agric.* **2020**, *173*, 105330. [[CrossRef](#)]
25. Liu, T.H.; Nie, X.N.; Wu, J.M.; Zhang, D.; Liu, W.; Cheng, Y.; Zheng, Y.; Qiu, J.; Qi, L. Pineapple (*Ananas comosus*) fruit detection and localization in natural environment based on binocular stereo vision and improved YOLOv3 model. *Precis. Agric.* **2022**, *23*, 1–22.
26. Liu, T.H.; Liu, W.; Zeng, T.J.; Qi, L.; Zhao, W.F.; Cheng, Y.F. Design and experiment of multi-flexible fingered roller pineapple harvesting mechanism. *Trans. Chin. Soc. Agric. Eng.* **2022**, *24*, 64–70, 38, 21–26.
27. Burks, T.; Villegas, F.; Hannan, M.; Flood, S.; Sivaraman, B.; Subramanian, V.; Sikes, J. Engineering and horticultural aspects of robotic fruit harvesting: Opportunities and constraints. *Hort Technol.* **2005**, *15*, 79–87. [[CrossRef](#)]
28. Thavamani, P.; Bhowmick, A.K. Wear of tank track pad rubber vulcanizates by various rocks. *Rubber Chem. Technol.* **1992**, *65*, 31–45. [[CrossRef](#)]
29. Howell, L.L.; Midha, A.J. A method for the design of compliant mechanisms with small-length flexural pivots. *J. Mech. Des.* **1994**, *116*, 280–290. [[CrossRef](#)]
30. Qi, H.J.; Joyce, K.; Boyce, M.C. Durometer hardness and the stress-strain behavior of elastomeric materials. *Rubber Chem. Technol.* **2003**, *76*, 419–435. [[CrossRef](#)]
31. Du, X.; Yang, X.; Ji, J.; Jin, X.; Chen, L. Design and Test of a Pineapple Picking End-effector. *Appl. Eng. Agric.* **2019**, *35*, 1045–1055. [[CrossRef](#)]
32. Liu, J.; Li, Z.; Li, P. Mathematical Modeling of Speedy Damage-Free Gripping of Fruit. In *Rapid Damage-Free Robotic Harvesting of Tomatoes*; Springer: Singapore, 2021; pp. 247–275.
33. Guo, A.F.; Li, J.; Guo, L.Q.; Jiang, T.; Zhao, Y.P. Structural design and analysis of an automatic pineapple picking and collecting straddle machine. In *Journal of Physics: Conference Series*; IOP Publishing: Bristol, UK, 2021; Volume 1777, p. 012029.
34. Anh, N.P.T.; Hoang, S.; Van Tai, D.; Quoc, B.L.C. Developing robotic system for harvesting pineapples. In Proceedings of the 2020 International Conference on Advanced Mechatronic Systems (ICAMEchS), Hanoi, Vietnam, 10–13 December 2020; pp. 39–44.
35. Fu, M.; Li, C.X.; Zheng, Z.Q. Design and analysis of semi-automatic screw type pineapple picking-collecting machine. *Chin. J. Eng. Des.* **2020**, *27*, 487–497.
36. Ma, X.Z.; Lian, H.S.; Gong, M.F.; Cheng, H.L.; Liao, G.X.; Deng, Z.X. Structural design and experiment of pineapple picking manipulator. *J. Shandong Agric. Univ. (Nat. Sci. Ed.)* **2020**, *51*, 727–732.